ACS Biomaterials SCIENCE & ENGINEERING

pubs.acs.org/journal/abseba
Article

Fabrication of Multiscale, Multidirectional Orientated Collagen Hydrogels with Guided Cell Alignment Using Fluidics and a Three-Dimensional Printing

Mizuki Iijima, Mitsuki Sato, Hoshi Wakabayashi, Kaori Kojima, Kanata Togashi, Shogo Oishi, Takumi Misu, Masaru Mukai, Hiroki Miyajima, Shoji Maruo, and Kazutoshi Iijima*

Cite This: ACS Biomater. Sci. Eng. 2025, 11, 2875−2887

Read Online

ACCESS | Metrics & More | Article Recommendations | Supporting Information

ABSTRACT: Various tissues have oriented collagen structures that confer mechanical strength and stability. However, creating models that precisely mimic the size and direction of these tissues remains challenging. In the present study, we developed a collagen tissue with multiscale and multidirectional controlled orientation using fluidic devices prepared using three-dimensional (3D) printing technology. Two types of fluidic channels were fabricated: a one-directional "horizontal orientation model" and vertical protrusions added to create a two-directional "vertical/horizontal orientation model". A type I collagen solution, mixed with or without cells, was introduced into the fluidic channel and gelled. As a result, in the horizontal orientation model, collagen fibrils and fibers were oriented by the flow. Both the fibroblasts and stem cells were aligned parallel to the flow along the collagen structure. In the vertical/horizontal orientation model, both the horizontal and vertical parts confirmed the orientation of collagen fibrils, fibers, and fibroblasts in both directions. Observation of the model at the nanoscale level using scanning electron microscopy (SEM) can explain the collagen orientation mechanism at the molecular and fibril levels. Prior to full gelation, collagen molecules and fibrils align parallel to the flow owing to the influence of flow and channel wall effects. This wall effect, starting from the outer channel wall, creates a gelated collagen "wall" toward the inside of the channel. Collagen fibrils aggregate into collagen fibers. In our experiments focusing on collagen contraction, the cell orientation was also described. As cells proliferate in response to the contact guidance of collagen fibrils and fiber orientation, focal adhesions and F-actin are activated and organize anisotropic traction forces that, in turn, drive cell orientation. Therefore, our method enables the customization of models with the desired tissue-specific orientations, thereby advancing future possibilities in tissue engineering.

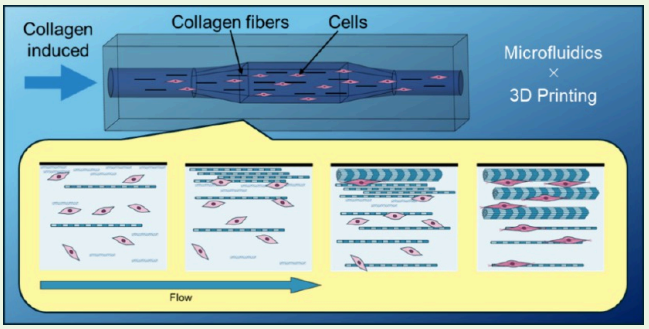

KEYWORDS: *orientated scaffold, collagen hydrogel, fluidics, three-dimensional printer, microfabrication*

1. INTRODUCTION

Collagen is the most prevalent protein in human tissues.[1] To date, 29 different collagen species have been reported,[2] several of which contribute to the formation and maintenance of the extracellular matrix (ECM) by assembling into larger structures.[1] These tissue-specific geometries provide tensile strength and mediate cell migration, growth, and differentiation.[3,4] Type I collagen, in particular, is abundant in the skin, bones, tendons, and ligaments, comprising approximately 90% of the collagen in human tissues.[5] Type I collagen exists as a triple-helix chain consisting of two α1 chains and one α2 chain.[5] The rod-like collagen molecule, which has a length of 300 nm and a diameter of 1.5 nm, self-organizes into fibrils of approximately 100 nm in diameter.[6] These fibrils aggregate further to form fibers and fiber bundles with diameters ranging from 1 to 20 μm.[6,7]

Oriented collagen structures have been observed in the skin,[8] bones,[9] tendons, and ligaments,[10] which confer mechanical strength and stability to tissues. In tendons and ligaments, collagen fibrils orient horizontally;[10] in the bone, particularly in the skull, flat bones show a two-dimensional (2D) orientation.[11] For the skin, collagen fibril and fibers in the dermal layer have two directions: papillary dermis with a vertical orientation and reticular dermis with a horizontal orientation.[8] The papillary dermis, with a thickness of 100−200 μm, contains thinner collagen fibrils and fibers, whereas

Received: November 15, 2024
Revised: March 28, 2025
Accepted: April 7, 2025
Published: April 19, 2025

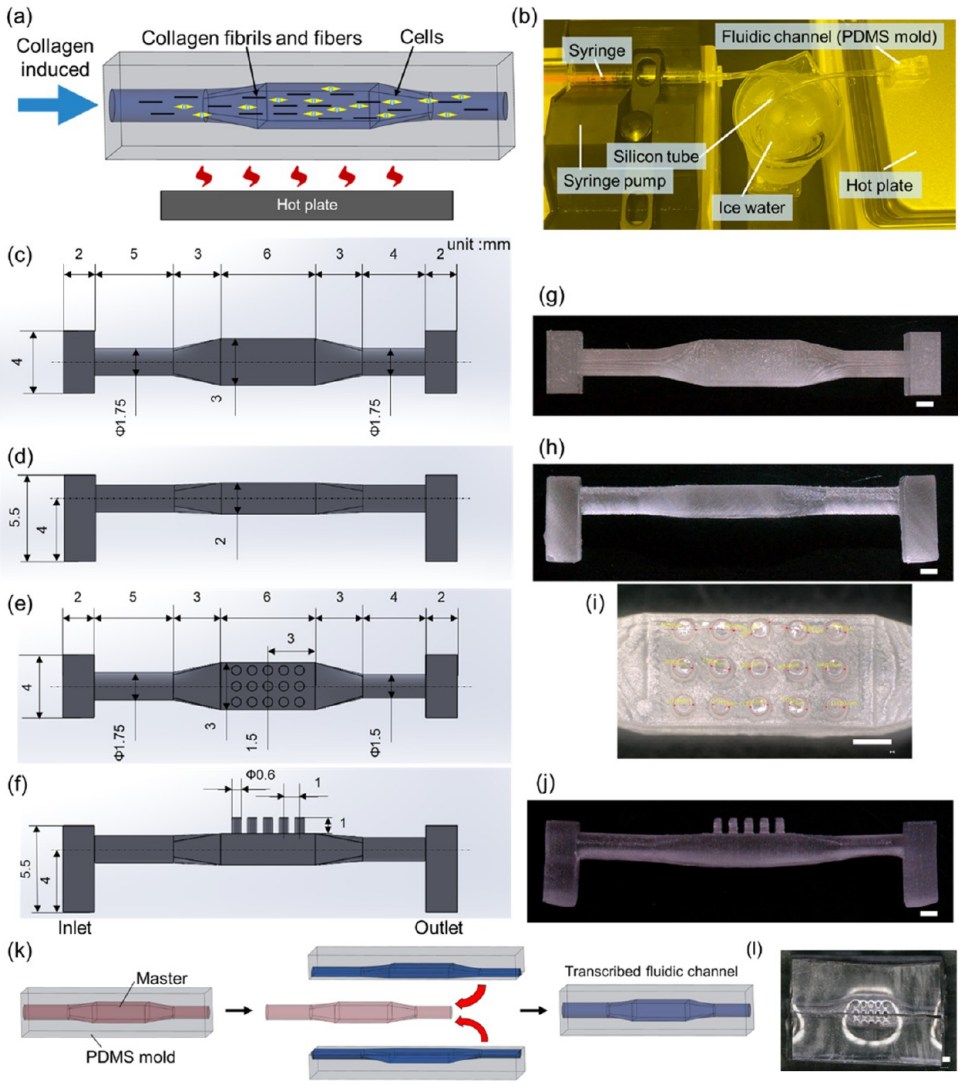

Figure 1. Schematic diagram of creating oriented collagen models. Overview of the experimental procedure showing collagen fibrils, fibers, and cell orientations induced by flow (a). Experimental image of the collagen solution induced by the syringe pump in the fluidic channel (b). Design of master (c–f) and microscopic images of actual masters made using a 3D printer (g–j) in horizontal orientation model (c, d, g, and h) and vertical/horizontal orientation model (e, f, i, and j); top view (c, e, g, and i) and side view (d, f, h, and j). Schematic diagram of PDMS fluidic channels formed by the master of horizontal orientation model (k) and macroscopic image of actual PDMS mold after being cut of vertical/horizontal orientation model (l). Scale bars: 1 mm.

the reticular dermis, with a thickness of 1000–4000 μm, is dominated by thicker collagen fiber bundles.[12] Thus, the collagen orientation in tissues is organized and functions on different scales and directions.

The orientation of collagen bundles affects cell behavior and function,[13,14] highlighting the importance of fabricating oriented collagen hydrogels as scaffolds. Several approaches exist for the construction of oriented collagen hydrogels. These methods include magnetic alignment,[15,16] electrospinning,[17] and stretching.[18,19] Oriented collagen hydrogels align neurons,[15,16] fibroblasts,[18] and myoblasts[19] along collagen hydrogels. This phenomenon of cells aligning along geometrical patterns is known as "contact guidance".[20] However, each method presents several challenges. Magnetic alignment uses magnetic beads that remain in the model.[15,16] Electrospinning requires volatile organic solvents that can destroy the structure of the three-stranded helix in collagen.[17] Stretching necessitates expensive machinery and specialized techniques, and it is also difficult to achieve multidirectional fine orientation.[18,19] However, microfluidics[21−24] has also been reported as a useful method for fabricating microscale collagen hydrogel-oriented models by injecting an initial flow into the channel. The conditions and principles of collagen bundle orientation have been investigated,[21,22] and aortic endothelial cells,[22] keratocytes,[23] and tenocytes[24] have been shown to grow and orient along oriented collagen hydrogels. Microfluidic methods can fabricate oriented models using only collagen and are inexpensive and easy to fabricate without toxicity or contamination risks. However, it is challenging to mimic complex-oriented structures such as the skin dermis or skull bone with two-directional orientations because of the immaturity of channel chip technology.

In this study, by including three-dimensional (3D) printing technology with channel fabrication, we developed a fluidic method for controlling the size and direction of oriented collagen hydrogels, thereby accurately recreating fine tissue fabrication. First, we controlled the orientation of both collagen and cells horizontally (one-directional) by mixing a

https://doi.org/10.1021/acsbiomaterials.4c02156
ACS Biomater. Sci. Eng. 2025, 11, 2875−2887

type I collagen solution with cells in a fluidic channel prepared from a master mold fabricated by using a 3D printer (Figure 1a,b). Under these optimized conditions, we developed a model that achieved a fine micro-oriented structure of both collagen and cells in the horizontal and vertical directions required in multidirectionally oriented tissues, such as skin. Subsequently, the obtained 3D collagen models were analyzed, and collagen formation and cell orientation mechanisms were investigated.

2. MATERIALS AND METHODS

2.1. Reagents. The collagen gel culture kit was purchased from Nitta Gelatin Co., Ltd. (Osaka, Japan). The kit contained 3 mg/mL collagen solution (Cellmatrix Type I-A, pig tendon, pH 3.0), 10× Ham's medium, and 50 mM reconstitution buffer (NaOH solution containing 260 mM $NaHCO_3$ and 200 mM 4-(2-hydroxyethyl)-1-piperazineethanesulfonic acid (HEPES buffer). Tween-20 was purchased from Thermo Fisher Scientific Inc. (Waltham, MA, USA). Tris(hydroxymethyl)aminomethane (Tris) and NaCl were purchased from Nacalai Tesque, Inc. (Kyoto, Japan). Ultrapure water was prepared using a Direct-Q UV3 (Merck Millipore, Burlington, MA, USA).

2.2. Cell Culture. Mouse embryonic fibroblast NIH3T3 cells (American Type Culture Collection [ATCC], Virginia, USA) and primary human bone marrow-derived mesenchymal stem cells (MSCs; Promocell, Heidelberg, Germany) were cultured in Dulbecco's modified Eagle's medium (D-MEM; Nacalai Tesque, Inc.) containing 10% fetal bovine serum (FBS; Thermo Fisher Scientific Inc.), and 1% of penicillin (100 U/mL)/streptomycin (100 μg/mL) solution (Nacalai Tesque, Inc.). The cells were cultured under 5% CO_2 humidity and a 37 °C temperature.

2.3. Simulation of Flow inside the Fluidic Channel. 3D simulations of the flow of the collagen solution inside the fluidic channel were performed using the COMSOL Multiphysics simulation (6.2 software). The flow channel geometry was designed using SolidWorks 3D computer-aided design (CAD) software (SP02.1) and imported into COMSOL. The physical parameters of each simulation were as follows: density, 1015 kg/m^3 (using the average value obtained from three measurements of 1 mL of collagen solution weight); viscosity, 120 mPa s (measured viscosity of the collagen solution was used; Figure S1); temperature, 20 °C.

2.4. Fabrication of Fluidic Channel. *2.4.1. Preparation of the Master Fluidic Channel.* Two types of orientation models were fabricated: a one-directional "horizontal orientation model", and vertical protrusions added a two-directional "vertical and horizontal (vertical/horizontal) orientation model". The master for each model was designed as shown in the following figures (horizontal orientation model: Figure 1c,d; vertical/horizontal orientation model: Figure 1e,f) using SolidWorks software and imported into Form 2 (Formlabs Inc., MA, USA), a high-resolution stereolithography 3D printer, for precise detailing. A stereolithography apparatus (SLA), the vat-photopolymerization technique, was used to fabricate the master. The master was created by layering horizontally with a layer pitch of 0.05 mm. Clear V4 Resin (RS-F2-GPCL-04, Formlabs, Inc.) was used as the master material. Supporting parts of the master were determined by using the automatic support generation function of the dedicated software "Preform" (Formlabs Inc.). After being molded, the resin was washed with isopropyl alcohol (IPA; FUJIFILM WAKO Pure Chemical Industries Ltd., Osaka, Japan) for 20 min, and the remaining IPA was removed using a blower. Then, the master was placed in a postexposure system, Form Cure device (FH−CU-01, Formlabs Inc.) at 60 °C for 15 min. The supports were then carefully removed by using diagonal pliers. The completed master is shown in Figure 1g,h (horizontal orientation model) and Figure 1i,j (vertical/horizontal orientation model).

2.4.2. Preparation of the Polydimethylsiloxane (PDMS) Mold (Fluidic Channel). A fluidic channel was fabricated using PDMS. The PDMS mold was fabricated by using a silicon potting material (Silpot 184, Toray Dow Corning, Co., Ltd., Tokyo, Japan) mixed with a curing agent at a 15:1 weight ratio. For the horizontal orientation model, the prepared master was placed in a polystyrene square case (PS CASE No.2, ASONE Co., Ltd., Osaka, Japan), and a silicon potting material was poured over the master. For the vertical/horizontal orientation model, the master was placed such that the protrusions faced upward, and the silicon potting material was poured into the case, enabling the protrusions to protrude slightly from the liquid surface. To remove the air bubbles, the encased PDMS mold was placed under a vacuum for 15 min. Thereafter, it was placed in a drying machine (60 °C, Programmable Gravity Convection Oven, DVS402; Yamato Scientific Co., Ltd., Tokyo, Japan) overnight for curing. Using a scalpel, the PDMS mold was cut horizontally when creating the horizontal orientation model (Figure 1k), and the PDMS mold was cut vertically when creating the vertical/horizontal orientation model (Figure 1l). Macroscopic images of the master PDMS mold were obtained by using a digital microscope (VHX-5000, Keyence Corp., Osaka, Japan) equipped with a high-performance low-magnification zoom lens (VHX-J20U; Keyence Corp.).

2.5. Preparation of Collagen Models. *2.5.1. Models without Cells.* For this model, 1.2 mL of 3 mg/mL collagen solution, 0.15 mL of Ham's medium, and 0.15 mL of reconstitution buffer were mixed at 4 °C (final collagen concentration: 2.4 mg/mL) and poured into a 1.0 mL syringe (Terumo Corp., Tokyo, Japan). The syringe was placed in a syringe pump (210 Legacy; KD Scientific Inc., MA, USA). This was connected to a PDMS mold placed on a hot plate stirrer (Rexim RSH-4DN, ASONE Co., Ltd.) with a 20 cm tube (Tygon LMT-55, Saint-Gobain, Tokyo, Japan). The tube was placed on ice to maintain the temperature at 4 °C (Figure 1b). After the syringe was manually pressed to fill the PDMS mold with collagen, collagen was poured through a syringe pump at 3 mL/h (syringe pump diameter, 4.58 mm; volume, 0.5 mL) and kept on a hot plate stirrer (Figure 1b). The collagen gel was then allowed to gel for 10 min. Thirty minutes after initiating flow using a syringe pump, the models were collected and incubated while immersed in the culture medium in a CO_2 incubator (5% CO_2 humidity and 37 °C temperature). During incubation, the culture medium was changed every 2−3 days. The model incubated in the PDMS mold was termed the With Mold (WM) model, and the model removed from the PDMS before incubation was termed the No Mold (NM) model. When these models were prepared using a syringe pump, they were termed the With Flow (WF) model, and when they were prepared without using a syringe pump but by pipetting 200 μL of collagen mixture directly into the PDMS mold, they were termed the No Flow (NF) model.

2.5.2. Models with Cells. For cell culture, 1.2 mL of 3 mg/mL collagen solution, 0.15 mL of Ham's medium, and 0.15 mL of reconstitution buffer were mixed with NIH3T3 cells or MSCs at 1.0 × 10^6 cells/mL at 4 °C (final collagen concentration: 2.4 mg/mL) and poured into a 1.0 mL syringe and placed in the syringe pump. The procedure of flowing collagen using a syringe pump follows the same steps as described in the "2.5.1. Models without cells" protocol.

2.6. Scanning Electron Microscopy (SEM) Observations. Treatment before supercritical drying was performed as previously described, with some modifications.[25] The fabricated cell-free collagen models were continuously immersed in IPA/water mixtures (25, 50, 75, and 100 vol %). The supercritical dryer (SCRD4; Rexxam Co. Ltd., Osaka, Japan) was precooled to 4 °C. The vessel in the model dryer was then immersed in IPA. The machine then performed supercritical drying (30 mL/min, 40 °C) with a back pressure valve (BPV) at 12 (90 min), 8 (10 min), and 0 MPa (40 min). After coating with Au for 20 s using a Quick Coater (MSP-1S; Vacuum Device Inc., Ibaraki, Japan), the samples were observed by using SEM (SU8010; Hitachi Ltd., Tokyo, Japan).

2.7. Immunofluorescence (IF) Staining of Collagen and Cell Morphology. Collagen was stained for type I. The model was removed from the culture medium and placed in 1.5 mL microtubes. The models were washed with phosphate-buffered saline (PBS (−); Nacalai Tesque, Inc.) and fixed with a 4% paraformaldehyde phosphate buffer solution (Nacalai Tesque, Inc.) for 10 min. After washing three times with PBS (−), they were exposed to 1% bovine serum albumin (BSA; Sigma-Aldrich Co. Ltd., MO, USA)-0.02%

https://doi.org/10.1021/acsbiomaterials.4c02156
ACS Biomater. Sci. Eng. 2025, 11, 2875−2887

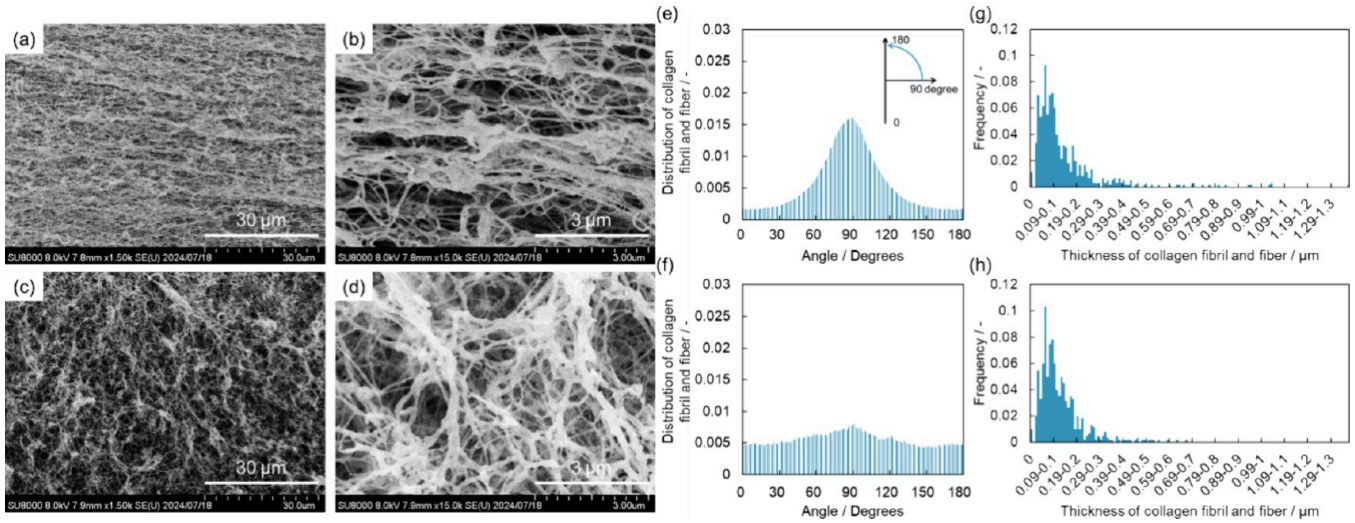

Figure 2. SEM observation and characterization of collagen fibrils and fibers in cell-free collagen hydrogel models. (a–d) SEM images of cell-free collagen hydrogels dried with IPA and CO_2 of WF (a, b) and the NF (c, d) model with 1500× (a, c) and 15,000× (b, d) magnifications. The angle of collagen fibril and fiber distribution of WF (e) and NF (f) model plotted at the range 0–180°. The flow direction coincides with the horizontal direction of the SEM image (90°). Distribution of the thickness of collagen fibril and fiber in the WF model (g) and NF model (h).

Tween 20-Tris-buffered saline (T-TBS, prepared from 0.5 M Tris, 1.4 M NaCl and 0.02% Tween-20, pH 7.4) solution for 3 min to block nonspecific adsorptions. The models were immersed in primary antibodies (1:100, Anti-Collagen I alpha 1, NB600-450, Novus Biologicals Ltd., Littleton, CO, USA) for 1 h at 25 °C. After exposure to 1%BSA-0.02%T-TBS twice for 5 min each time, the models were further immersed in a secondary antibody (1:100, fluorescein isothiocyanate [FITC]-conjugated goat antirabbit IgG, ab6785, Abcam Ltd., Cambridge, UK) for 1 h at 25 °C under light-shielding conditions. The cells were washed twice with PBS (−) for 5 min each time. The models without cells were placed on a glass slide and observed using a fluorescence microscope (Leica DMI3000 B; Leica Microsystems Inc., Nussloch, Germany). To observe the models with cells, cells were stained for filamentous actin (F-actin) and nuclei after collagen staining. The cells were permeabilized with 0.5% Triton solution (Sigma-Aldrich) for 10 min and washed three times with PBS (−). The models were eventually stained with 100 nM rhodamine-phalloidin (Fujifilm Co., Ltd., Tokyo, Japan) in PBS (−) for 40 min to label F-actin under light-shielding conditions. After washing three times with PBS (−), the cells were stained with 100 nM DAPI (Dojindo Laboratories Co., Ltd., Kumamoto, Japan) in PBS (−) to label the nuclei under light-shielding conditions. After washing three times with PBS (−), the models were placed on glass slides and observed using fluorescence microscopy. The vertical/horizontal orientation models for IF staining were examined by using a motorized zoom microscope (Axio Zoom.V16, Zeiss, Jena, Germany).

2.8. Qualification of the Thickness of Collagen Fibrils and Fibers. Two hundred points of collagen fibrils and fiber thickness in each image were manually measured by setting scales using ImageJ software.

2.9. Qualification of the Orientation of Collagen and Cells. ImageJ 1.54i–1.54k software with a Java plugin OrientationJ[26] was used in 15,000× and 80,000× SEM images for collagen orientation. After making the background transparent with "Threshold", the orientation of the collagen fibril and fiber was quantified with the "Riesz Filter" of the OrientationJ Distribution (Figure S2). For the vertical/horizontal orientation model, two locations were quantified for each protrusion and main part, and the averages of the two models were calculated. For all other models, three locations were quantified for each model, and the average of the three models was calculated.

For the cell orientation, "Fit ellipse" in ImageJ was used. After making the background transparent with "Threshold," the orientation of the cells was quantified as the angle of the major axis of the approximate ellipse using 'Analyze particles' (Figure S3). For the vertical/horizontal orientation model, three locations were quantified for each protrusion and main part, and the averages of the three models were calculated.

2.10. Statistical Analysis. The results are presented as the mean ± standard deviation (SD). All statistical analyses were performed using EZR software (version 1.68, Saitama Medical Center, Jichi Medical University, Saitama, Japan), a graphical user interface for R.[27] Statistical significance was tested using Student's t test for samples that followed a normal distribution and Kruskal–Wallis with Steel-Dwass post hoc multiple comparison test for samples that did not follow a normal distribution (all test significance levels were set at $p < 0.05$). All experiments were repeated at least three times.

3. RESULTS

3.1. Computational Simulation of Flow in the Fluidic Channel Using COMSOL. We investigated whether the entire fluidic channel path exhibited a laminar flow, considering the velocity distribution of the flow in the fluidic channel, by varying the inlet velocity conditions using computational fluid dynamics (CFD) simulations in COMSOL. Four inlet flow rates (1, 3, 6, and 125 mL/h) up to the maximum flow rate of the syringe pump were examined (Figures S4–S7). Based on the velocity distribution, the flow proceeds smoothly throughout the channel at all four inlet flow rates (Figures S4a, S5a, S6a, and S7a). From the stream distribution, all arrow directions (arrow lengths: flow velocity; arrow direction: flow direction; colors: velocity distribution according to flow velocity) pointed toward the outlet without twisting, indicating that the flow can be considered laminar (Figures S4b,c, S5b,c, S6b,c, and S7b,c). The velocities at three points in the z-axis (defined as the distance from the entrance; α: 9.0 mm, β: 11.0 mm, γ: 13.0 mm, $y = 0$) are shown in Figures S4d, S5d, S6d, and S7d. Because the velocities at the three points showed no significant differences, all four conditions were laminar with no turbulence. In addition, the velocity at the center of the model was higher than that at the channel walls (Figures S4d, S5d, S6d, and S7d).

3.2. Analysis of the Collagen Fiber Orientation. To examine the collagen fiber orientation in a cell-free collagen model, the fabricated collagen hydrogels dried with IPA and supercritical CO_2 of the WF and NF models were observed

https://doi.org/10.1021/acsbiomaterials.4c02156
ACS Biomater. Sci. Eng. 2025, 11, 2875–2887

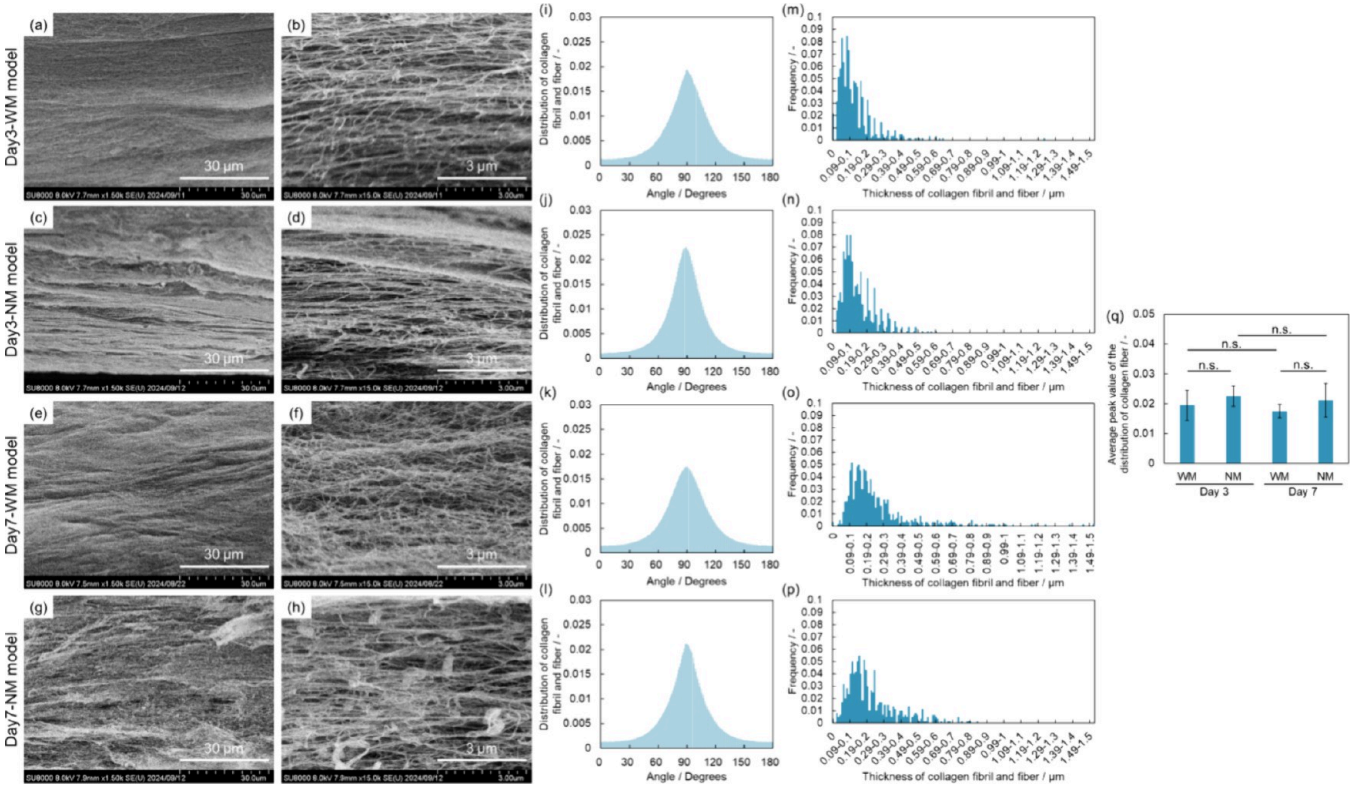

Figure 3. SEM observation and characterization of collagen fibrils and fibers in cell-free collagen hydrogel models after immersion in PBS (−) for 3 and 7 days. (a−h) SEM images of cell-free collagen hydrogels of WM (a, b, e, and f) and NM (c, d, g, and h) dried with IPA and CO_2 after immersion in PBS (−) for 3 (a−d) and 7 days (e−h) with 1500× (a, c, e, and g) and 15,000× (b, d, f, and h) magnifications. The angle of collagen fibril and fiber distribution in cell-free collagen hydrogels of WM (i, k) and NM (j, l) dried with IPA and CO_2 after immersion in PBS (−) for 3 (i, j) and 7 days (k,l) plotted at the range 0−180°. The flow direction coincides with the horizontal direction of the SEM image (90°). Distribution of the thickness of collagen fibril and fiber in cell-free collagen hydrogels of WM (m, o) and NM (n, p) dried with IPA and CO_2 after immersion in PBS (−) for 3 days (m, n) and 7 days (o, p). The average peak value of the angle distribution of collagen bundles (q), (* $p < 0.05$).

using SEM (Figure 2a−d). First, the orientation of collagen fibrils and fibers was quantified. In the WF model, collagen fibrils and fibers were oriented in the same direction as the flow (Figure 2a,b,e). In contrast, in the NF model, the collagen fibrils and fibers were randomly oriented (Figure 2c,d,f). The average peak values for the angle of collagen fibril and fiber distribution were higher in the WF model than in the NF model (WF: 0.0161 ± 0.0026, NF: 0.0080 ± 0.0032; Figure 2e,f).

The width of the collagen bundles was quantified. The collagen bundles with thin (≈100 nm) and thick (−1 μm) fibers were observed in both the WF and NF models (Figure 2b,d). The width of thin collagen bundles corresponds to collagen fibril (100 nm), and thick collagen bundles correspond to collagen fiber (1−20 μm).[6] The distribution of the thickness of the collagen bundles is shown in Figure 2g,h. The WF and NF models had a mode of 50−60 nm (frequency, WF model, 0.093; NF model, 0.103), which corresponded to the thickness of the collagen fibrils. The shoulder of the graph, detected at a thicker position in the WF model (approximately 120 nm), was thicker than that in the NF model (100 nm) (Figure 2g,h). Notably, the WF model showed a long-tailed distribution reaching fiber thicknesses of up to 1.37 μm, whereas the NF model reached up to 0.67 μm (Figure 2g,h). This indicates that the diameter of the collagen fibers in the WF model was greater than that in the NF model.

3.3. Investigation of Collagen Gel Orientation Retention. Next, to examine whether the collagen gel structure could be maintained during long-term culture, the orientation of the cell-free collagen gel after incubation in PBS (−) for 3 or 7 days was observed using SEM. Two types of models were prepared: those immersed in PBS (−) after being removed from the PDMS molds (no mold (NM) model) and those immersed in PBS (−) while still in the PDMS molds during incubation (with mold (WM) model) (Figure 3). The SEM images showed that the collagen bundles were oriented in the same direction as the flow in all models (Figure 3a−h). No significant difference in the average peak value of collagen bundle orientation was observed between days 3 and 7, irrespective of the presence or absence of mold (Figure 3i−l,q). When analyzing the collagen fibril and fiber thicknesses on day 3, the mode was 40−50 nm in the WM model (frequency: 0.083) and 70−80 nm in the NM model (frequency: 0.080), which was the fibril size (Figure 3m,n). On day 7, the mode was 100−110 nm in the WM model (frequency: 0.052) and 140−150 nm in the NM model (frequency: 0.055), which is the fiber size (Figure 3o,p). For both the WM and NM models, the mode was distributed to a thicker fiber size on day 7 than on day 3, and the overall distribution extended to a thicker fiber size on day 7, indicating that thicker fibers were observed on day 7. When the WM and NM models were compared on days 3 and 7, the mode was distributed in a thicker position in the NM model than in the WM model (Figure 3m−p). However, on days 3 and 7, the WM model showed a longer distribution than the NM model (Figure 3m−p). Day 3-WM reached fiber thicknesses of up to 1.23 μm, whereas day 3-NM

https://doi.org/10.1021/acsbiomaterials.4c02156
ACS Biomater. Sci. Eng. 2025, 11, 2875−2887

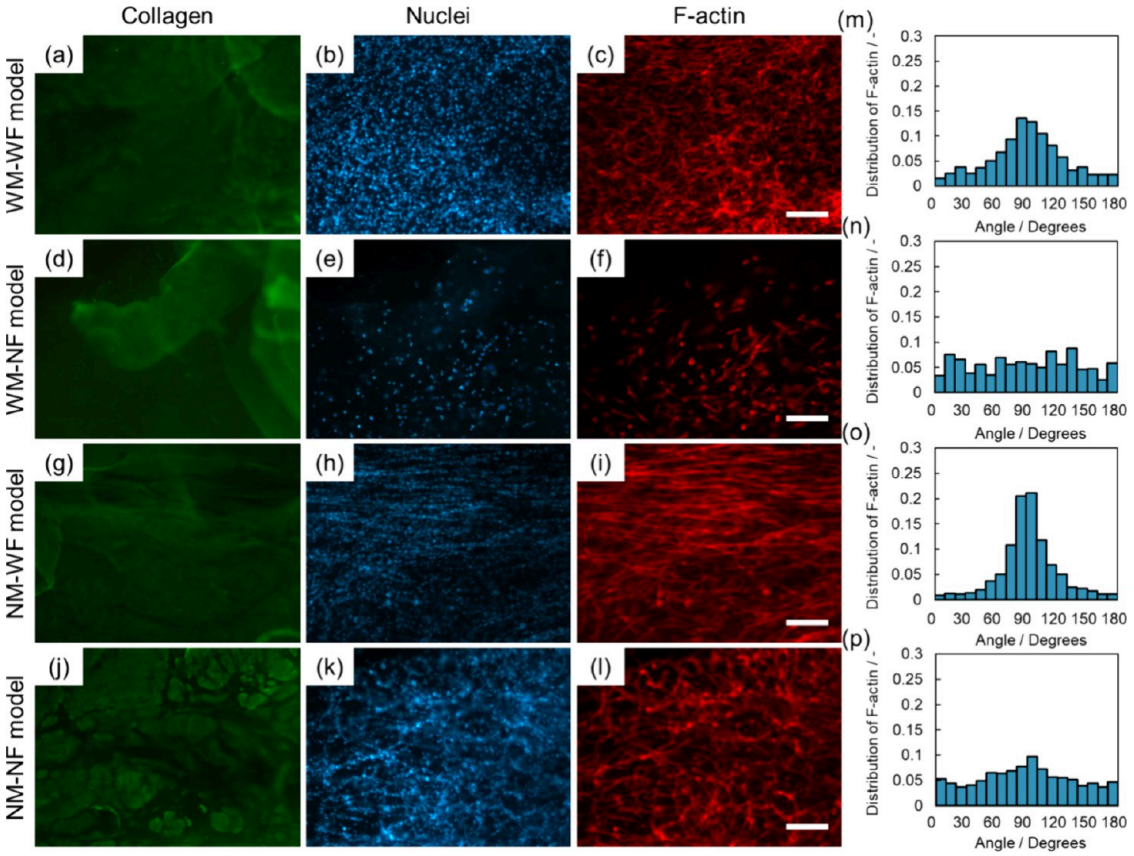

Figure 4. Fluorescence microscopic observation of collagen models with NIH3T3 after 3 days of culture. The models of WM-WF (a−c, m), WM-NF (d−f, n), NM-WF (g−i, o), and NM-NF (j−l, p) are shown. Fluorescence images staining collagen with antitype I collagen antibody (green, a, d, g, and j), nuclei with DAPI (blue, b, e, h, and k), and cytoskeletal protein F-actin with rhodamine-phalloidin (red, c, f, i, and l) after 3 days of culture. Scale bars = 200 μm. The flow direction coincides with the horizontal direction of the fluorescence image (90°); The angle of F-actin distribution was plotted at the range 0−180° (m, n, o, and p).

reached up to 0.60 μm, and day 7-WM reached fiber thicknesses of up to 1.52 μm, whereas day 7-NM reached up to 0.84 μm (Figure 3m−p). Combining the mode and distribution, we observed no significant differences in the distribution of collagen fibril and fiber thicknesses between the NM and WM models.

3.4. Morphological Observation and Analysis of the Cell Orientation in Collagen Hydrogels with NIH3T3 Cells. The cells were then embedded in a collagen hydrogel and cultured. Figure S8a shows macroscopic images of the collagen models with and without mouse embryonic fibroblast NIH3T3 cells on days 0 and 3. The length of the model with cells was predominantly reduced on day 3 (1.03 ± 0.13 mm) compared to day 0 (1.67 ± 0.13 mm) (Figure S8b). In contrast, the model without cells showed no significant difference in length (day 0 model 1.47 ± 0.13 mm, for the day 3 model 1.43 ± 0.01 mm; Figure S8b). Therefore, the model with cells was found to shrink significantly after 3 days of culture.

In the next experiment, to examine cell orientation, WF and NF models with or without mold were cultured for 3 days each, and cell morphology was compared by staining collagen with an antitype I collagen antibody, nuclei with DAPI, and F-actin with rhodamine-phalloidin (Figure 4a−l). For the WF model, both the WM and NM models had cell orientations directed in the same manner as the flow (Figure 4c,i). The WM and NM models had no cell orientation in the same direction as the NF model, and the cells were randomly placed (Figure 4f,l). The orientation of F-actin was also quantified (Figure 4m−p). The average peak values of F-actin distribution for the WM model, WF: 0.1358 ± 0.0102, NF: 0.0881 ± 0.0230 (Figure 4m,n), and for the NM model, WF: 0.2106 ± 0.0075, NF: 0.0971 ± 0.0089 (Figure 4o,p). The WF model exhibited values higher than those of the NF model for both the WM and NM models. When comparing the WF model to the WM and NM models, the NM model showed higher values than the WM model (Figure 4m,o).

3.5. Cell Orientation in Collagen Hydrogels with MSCs. In the next experiment, to examine the cell orientation of MSCs, WF and NF models with or without mold were cultured for 3 days each and compared in terms of cell morphology (Figure 5a−l). For the WF model, both the WM and NM models exhibited cell orientations directed in the same manner as that of the flow (Figure 5c,i). For the NF model, both the WM and NM models had no cell orientation in the same direction, and the cells were randomly placed (Figure 5f,l). The average peak values of F-actin distribution for the WM model, WF: 0.1726 ± 0.0111, NF: 0.0730 ± 0.0105 (Figure 5m,n), for the NM model, WF: 0.2404 ± 0.0249, NF: 0.0617 ± 0.0102 (Figure 5o,p). The WF model exhibited higher values than the NF model for both the WM and NM models. In the WF model, the NM model exhibited higher values than the WM model (Figure 5m,o).

https://doi.org/10.1021/acsbiomaterials.4c02156
ACS Biomater. Sci. Eng. 2025, 11, 2875−2887

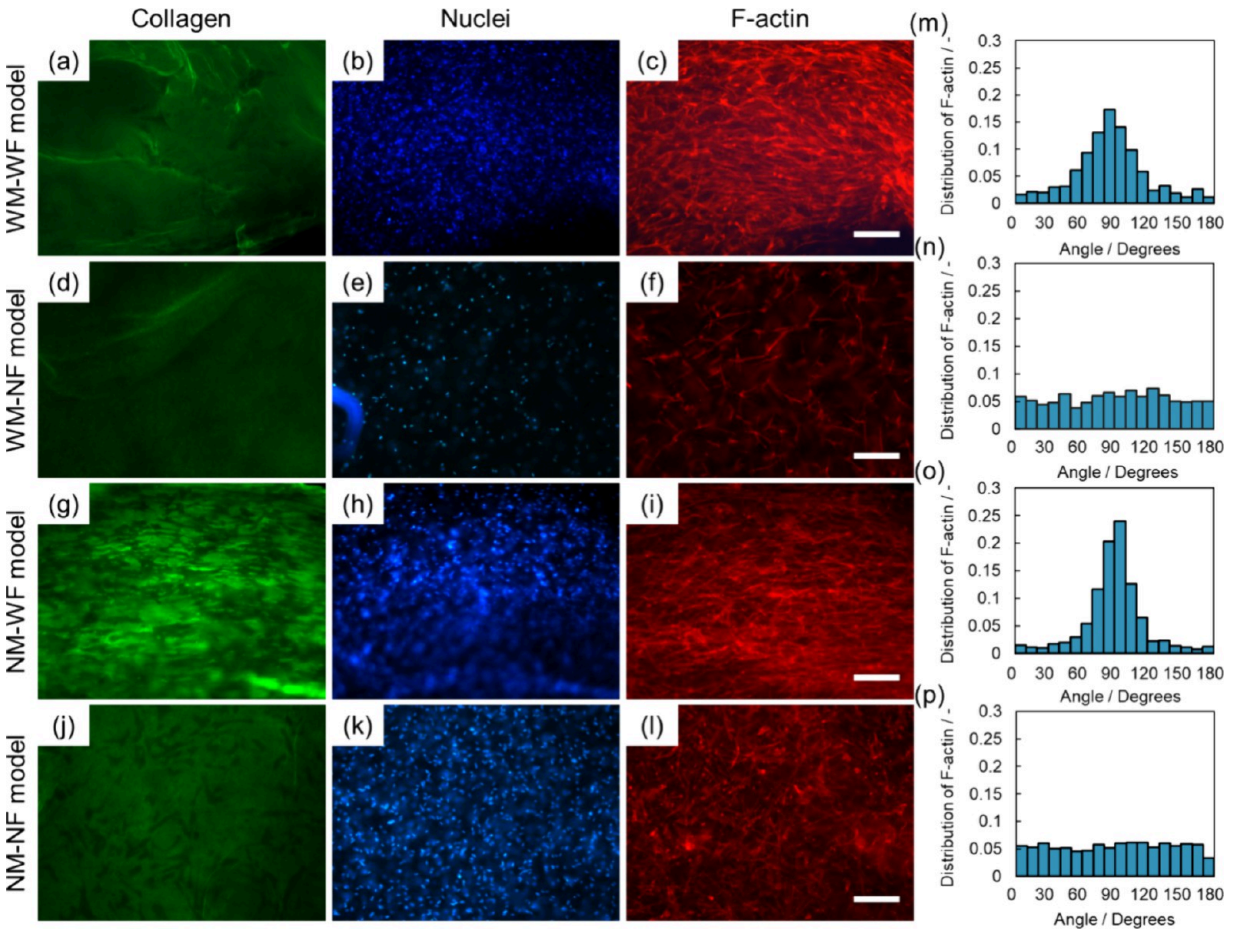

Figure 5. Fluorescence microscopic observation of collagen models with MSCs after 3 days culture. The models of WM-WF (a−c, m), WM- NF (d−f, n), NM-WF (g−i, o), and NM-NF (j−l, p) are shown. Fluorescence images staining collagen with antitype I collagen antibody (green, a, d, g, and j), nuclei with DAPI (blue, b, e, h, and k), and cytoskeletal protein F-actin with rhodamine-phalloidin (red, c, f, i, and l) after 3 days of culture. Scale bars = 200 μm. The flow direction coincides with the horizontal direction of the fluorescence image (90°); The angle of F-actin distribution was plotted at the range 0−180° (m, n, o, and p).

3.6. Fabrication of the Vertical/Horizontal Orientation Model. To create a vertical−horizontally oriented collagen model, a flow channel consisting of a horizontal channel with vertical cylindrical protrusion channels on top of the horizontal channel was designed (Figure 1e,f). By analyzing this vertical/horizontal orientation model using COMSOL, we confirmed that collagen flowed out in a laminar manner through the vertical protrusions and outlet in the simulations (Figure S9).

To examine the gel structure, collagen hydrogel models of WF and NF dried with IPA and supercritical CO_2 were observed by using SEM (Figure 6a−h). In the WF collagen hydrogel models, the collagen bundles were oriented vertically and horizontally in the vertical protrusion (Figure 6b) and the main parts of the hydrogel models (Figure 6d), respectively. In contrast, in the collagen hydrogel models of NF, the collagen bundles were randomly oriented in the vertical protrusion (Figure 6f) and the main parts (Figure 6h). The orientation of the collagen bundles was quantified (Figure 6i−l). The average peak values for the angle of collagen fibril and fiber distribution were WF model vertical protrusion part 0.0124 ± 0.0021 (Figure 6i), and WF model main part 0.0169 ± 0.0027 (Figure 6j). Therefore, the average peak values of the main part are higher than those of the vertical protrusion. For the NF model, the average peak values for the angle of collagen fibril and fiber distribution had no significant difference between the NF model vertical protrusion part, 0.0070 ± 0.0009 (Figure 6k), and in NF model main part, 0.0071 ± 0.0010 (Figure 6l). Both the vertical protrusion and main parts of the WF model had higher peak values than those of the NF model (Figure 6i−l).

When analyzing the collagen fibril and fiber thicknesses in the WF model, the modes of bundle thickness were 10−20 nm in the vertical protrusion part (frequency: 0.239) and 50−60 nm in the main part (frequency: 0.072) (Figure 6m,n), respectively. In the NF model, the modes were 30−40 nm in the vertical protrusion region (frequency: 0.133), and 90−100 nm in the horizontal region (frequency: 0.094) (Figure 6o,p). Therefore, in both the WF and NF models, thinner fibrils were observed in the vertical protrusions than in the main part. In the WF model, the shoulder of the graph appeared at a thicker position in the main part than in the vertical protrusion, which was approximately 30 nm in the main part and 140 nm in the vertical protrusion (Figure 6m,n). In the NF model, the shoulder of the graph appeared at a thicker position in the main part than in the vertical protrusion part, which was approximately 60 nm in the main part and 140 nm in the vertical protrusion (Figure 6o,p). Therefore, the main part formed a fiber that was thicker than the vertical protrusion in both the WF and NF models. When observing the main parts, where fiber grew noticeably, the WF model showed a long-

https://doi.org/10.1021/acsbiomaterials.4c02156
ACS Biomater. Sci. Eng. 2025, 11, 2875−2887

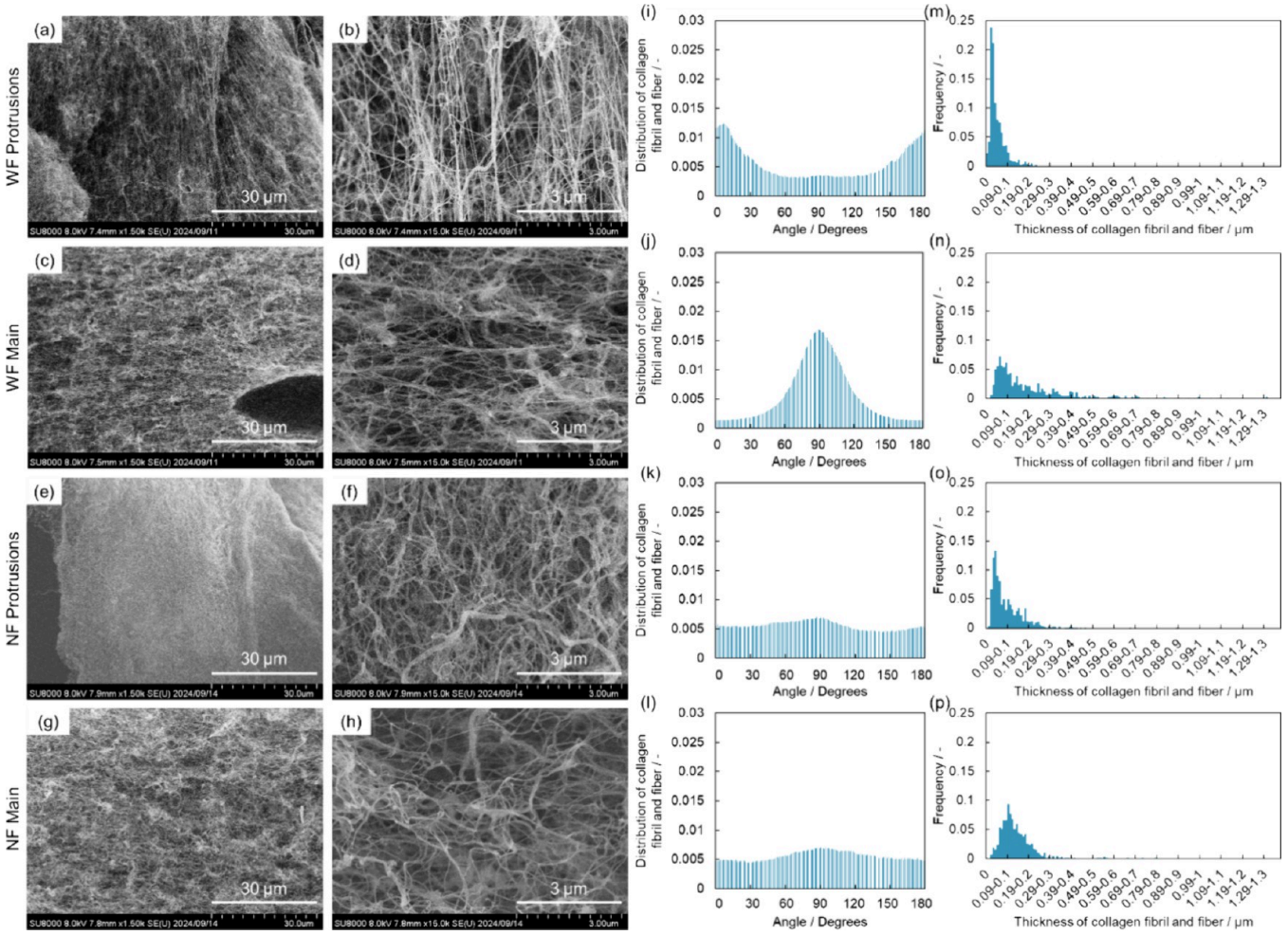

Figure 6. SEM observation and characterization of collagen hydrogels of a vertical/horizontal orientation model on day 0. (a–h) SEM images of collagen fibril and fiber of protrusion part (a, b, e, and f) and main part (c, d, g, and h) in WF models (a–d) and NF models (e–h) with a magnification of 1500× (a, c, e, and g) and 15,000× (b, d, f, and h). (i–l) Distribution of the thickness of collagen fibril and collagen fiber WF model protrusion part (i), WF model main part (j), NF model protrusion part (k) and NF model main part (l). (m–p) Angle of collagen fibril and fiber distribution of WF model protrusion part (m), WF model main part (n), NF model protrusion part (o), and NF model main part (p) plotted at the range 0–180°. The flow direction coincides with the horizontal direction of the SEM image (90°).

tailed distribution reaching fiber thickness of up to 1.31 μm, whereas the NF model reached up to 0.79 μm; therefore, the WF model showed thicker collagen fibers than the NF model (Figure 6n,p).

Next, NIH3T3 cells were embedded in vertical/horizontal orientation collagen models and cultured for 3 days. The vertical/horizontal orientation models were difficult to remove from the PDMS mold because of their insufficient strength; therefore, they were observed while being placed in the PDMS mold (Figure 7a–l). In the WF model, the cells within the vertical protrusion are oriented vertically (Figure 7c), whereas those in the main part are aligned horizontally (Figure 7f). This result was supported by the distribution of the F-actin orientation (Figure 7m–p). The average peak values for the angle of the F-actin distribution at the vertical protrusion part were 0.2098 ± 0.0577 (Figure 7m), and the average peak values at the main part were 0.1474 ± 0.0163 (Figure 7n). For the NF model, no specific orientation was observed in either the vertical protrusion or the main part (Figure 7i,l). The average peak values for the angle of the F-actin distribution at the vertical protrusion part were 0.0963 ± 0.0466 (Figure 7o), and at the main part, it was 0.0723 ± 0.0095 (Figure 7p).

4. DISCUSSION

This study used fluidic devices and 3D printing technology to develop collagen tissue that can control the size and direction of the collagen hydrogel and cell orientation.

Typically, a master for a fluidic channel is fabricated using photolithography,[24] soft lithography,[28] drilling-based injection molding,[29] or 3D printing.[30] However, photolithography and soft lithography are applicable only to flat substrates, making it difficult to realize 3D complex shapes than 3D printers.[24,28] Drilling-based injection molding processing can be three-dimensional but requires specialized knowledge to create complex structures, which is costly and time-consuming.[29] To fabricate master flow channels, we used 3D printing, which significantly reduces the time required for prototyping channel designs and allows for the simultaneous production of dozens of units, enabling rapid and convenient mold fabrication. Moreover, 3D printing, which allows for highly flexible designs suitable for 3D cell culture, can be used to create master molds with complex shapes. In particular, the vat polymerization techniques used in this study had the highest modeling accuracy among the 3D printing methods.[31] Therefore, our method allows for the precise and flexible fabrication of molds

https://doi.org/10.1021/acsbiomaterials.4c02156
ACS Biomater. Sci. Eng. 2025, 11, 2875–2887

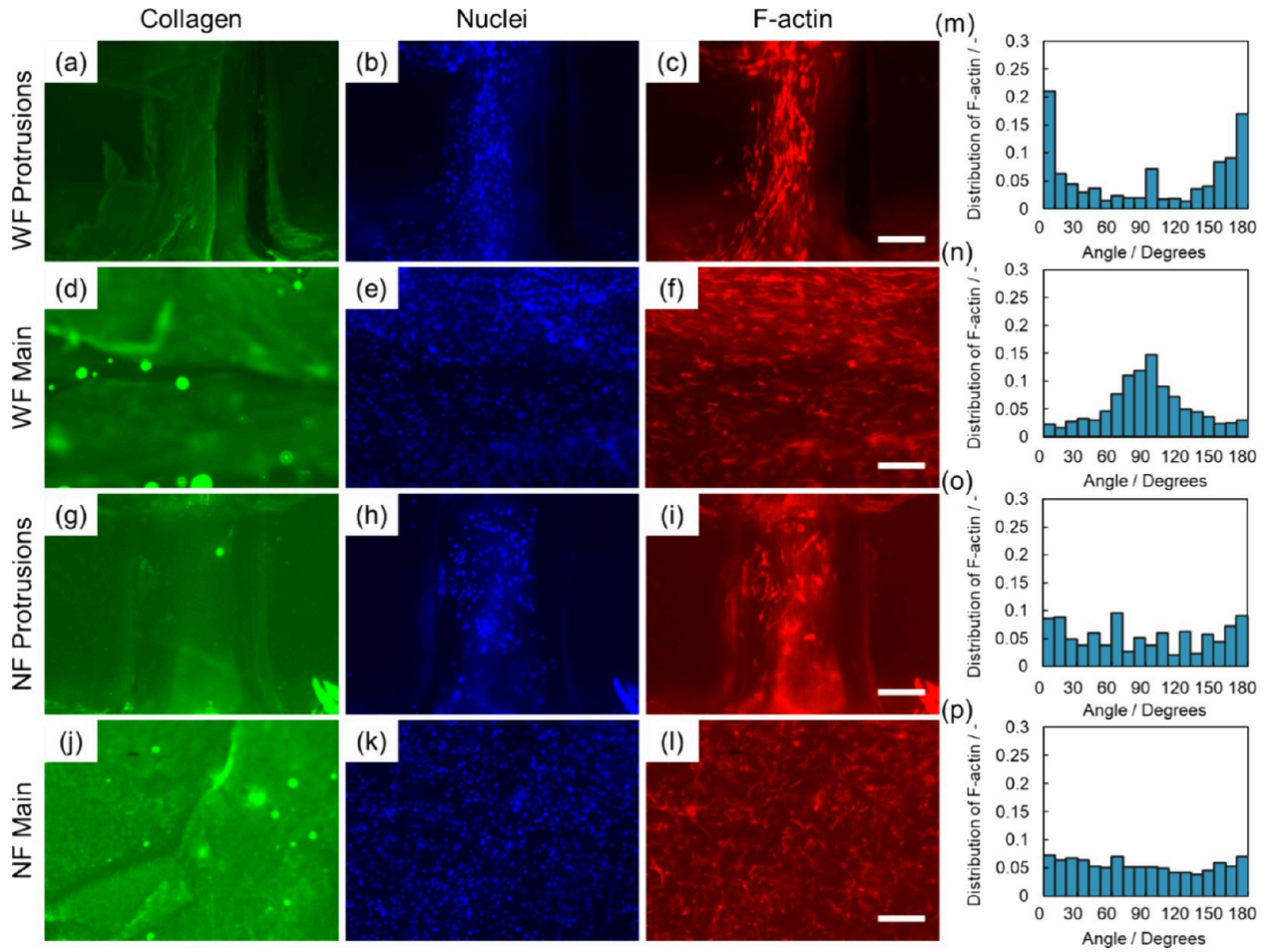

Figure 7. Fluorescence microscopic observation of vertical/horizontal orientation model with NIH3T3 after 3 days of culture. The models of the WF protrusion part (a–c, m), WF main part (d–f, n), NF protrusion part (g–i, o), and NF main part (j–l, p) are shown. Fluorescence images staining collagen with antitype I collagen antibody (green, a, d, g, and j), nuclei with DAPI (blue, b, e, h, and k), and cytoskeletal protein F-actin with rhodamine-phalloidin (red, c, f, i, and l) after 3 days of culture. Scale bars = 200 μm. The direction of flow coincides with the horizontal direction of the fluorescence image (90°); The angle of F-actin distribution was plotted at the range 0–180° (m, n, o, and p).

at the micrometer scale, which is required to mimic microstructures such as skin.

First, a computational method was used to validate the flow model. COMSOL can be used to simulate the detailed flow velocity distributions throughout the entire channel.[32] All four inlet flow rates (1, 3, 6, and 125 mL/h) were laminar with no turbulence (Figures S4–S7). Next, experiments were conducted to determine the optimal conditions for observing collagen orientation (Figure S10). Because the collagen fibers were subjected to sufficient shear stress to orient them at 3 mL/h (Figure S10c,d), this condition was used for the experimental system in this study.

SEM was used to numerically analyze the collagen bundle diameter and orientation to capture the fine structure of the collagen hydrogels (Figure 2). In the SEM images, collagen bundles were oriented in the flow direction in the WF model and randomly oriented in the NF model as controls, indicating that our fluidic channel model controlled the horizontal orientation of collagen (Figure 2a–f). Also, there was no significant difference between the WF and NF models in the size of fibrils (≤100 nm[6]); however, the WF model, with graph shoulders on the larger diameter size and more long-tailed distributed, was considered to form thicker fibers (>100 nm[6]) than the NF model (Figure 2g,h).

Based on these results, the mechanism of collagen orientation with flow was discussed. In a previous study by Lee et al., oriented collagen fibrils in fluidic channels with widths of ≤100 μm were obtained.[22] They argued that the orientation of collagen can be attributed to two factors: orientation due to flow and geometrical restriction of the channel walls.[22] It is likely that the flow effect on collagen occurred before it was completely gelatinized. By applying the flow, the rod-like triple-stranded helical collagen molecules aligned at the edge of the channel walls, and subsequent fibril polymerization occurred in the flow direction.[22] What was observed in all collagen SEM images was the center of the model, with a width of 3 mm and a height of 2 mm. In the Lee et al. study, under their experimental conditions, the results showed no orientation at widths larger than 100 μm, but other studies have shown that orientation occurs at widths as large as 2–3 mm,[21,33] which is consistent with our experiment results. Although collagen orientation has been observed in flow channel models with widths of 2–3 mm, the mechanism of collagen orientation at the center of the model has not yet been clarified. In our study, the channel wall first caused the collagen molecules and fibrils to orient near the wall surface and gel. This gelated collagen becomes the "wall" of collagen, to which the next collagen molecules and fibrils adhere, and

https://doi.org/10.1021/acsbiomaterials.4c02156
ACS Biomater. Sci. Eng. 2025, 11, 2875–2887

gradually, this effect continues outside toward the inside of the channel with the collagen "wall." This can be considered the mechanism through which the collagen is oriented at the central regions under the influence of the flow and the "walls." This was confirmed by the SEM images, which showed that the smallest collagen fibrils observed in the middle of the model appeared to be fixed in space and grew without strong bending (Figure 2b). This led to the fibrils being oriented by flow from one end attached to the wall and the other to a location of low hydrodynamic resistance to the flow, which was parallel to the flow direction.[21] As the fibrils continue to grow, collagen aggregates and thickens, becoming a strong fiber.[7] As significantly thicker collagen fibers were observed in the WF model compared to the NF model, whereas collagen fibrils were not significantly different, it is considered that collagen fibrils aggregate to form thicker collagen fibers during collagen orientation with the influence of the flow and the "walls" (Figure 2g). However, because the NF model was not affected by this flow, the neighboring fibrils were not parallel to each other, making it difficult to form thicker fibers, as in the WF model (Figure 2h).

Next, long-term incubation under collagen flow conditions in a cell-free environment was examined. Regardless of the presence or absence of mold, there were no significant differences in the orientation peak values after 3 and 7 days of incubation (Figure 3q), indicating that the orientation of collagen bundles in the collagen hydrogels was maintained over long-term incubation. Regarding the thickness of the collagen bundles, for both the WM and NM models, thicker fibers were observed on day 7 than on day 3, suggesting that once the fibrils developed into fibers, they continued to grow and strengthen during long-term incubation. In summary, this orientation model suggests that even during long-term incubation after gelation is complete, fibrils continue to aggregate and form thick fibers.

Cellular experiments were conducted using mouse embryonic fibroblast NIH3T3 cells and primary human MSCs. MSCs are known for their capacity to differentiate into various types of cells, such as osteoblasts, adipocytes, myoblasts, chondrocytes, and fibroblasts, rendering them valuable for tissue regeneration in humans.[34] Although both cell types are derived from the mesoderm, we attempted to demonstrate the validity of our method by evaluating cell orientation using fibroblasts and MSCs from different cell types.

After 3 days of culture, regardless of the presence or absence of the mold, both NIH3T3 cells and MSCs were oriented along the direction of flow in the WF model, whereas cells in the NF model showed a random orientation (Figures 4 and 5). Previous studies have shown that cell orientation is facilitated by contact guidance along the oriented collagen hydrogel.[20,22] Contact guidance induces the maturation of focal adhesions, the primary mechanosensors of cells, and the alignment of F-actin.[35−37] This process organizes anisotropic traction forces, which in turn drive cell orientation.[35,36] When cells enter the collagen matrix, cellular traction remodels the collagen structure.[38,39] In our experiments, the collagen hydrogels with cells prepared under flow conditions shrank remarkably compared to the cell-free collagen models (Figure S8). This result confirms that cells contribute to collagen hydrogel shrinkage, owing to cell traction forces.

Both NIH3T3 cells and MSCs in the NM models exhibited higher peak orientation values than those in the WM models under flow conditions (Figures 4 and 5). First, oxygen and nutrients were supplied more efficiently to cells cultured in collagen hydrogels than to those cultured in PDMS molds. Owing to the abundance of oxygen and nutrients, the environment is conducive to cell proliferation, which increases the cell density. An increased cell density results in strong cell contraction forces. Thus, with stronger cell contraction forces that resulted in a stronger cell orientation, the NM models had a higher cell orientation than the WM models.

Finally, we attempted to replicate the microstructures in the horizontal and vertical directions, similar to human skin. Collagen fibrils and fibers in the dermal layer of the human skin consist of a horizontal orientation and fine vertical orientation in papillary projections.[8] In the design of fluidic channels for vertical/horizontal orientation models, protrusions were first added to the horizontal orientation model design and simulated in COMSOL (Figure S11). Consequently, it was suggested that the velocity in the protrusion was too low. By reducing the outlet diameter from 1.75 to 1.50 mm and resimulating (Figure S9), the flow velocity in the protrusion part was almost the same as the flow velocity in the center of the device for the horizontal orientation model. Therefore, this design was used to create vertical/horizontal orientation models.

SEM and fluorescence images were used to examine the vertical/horizontal orientation models. The SEM images showed that collagen fibrils and fibers within the vertical protrusion were oriented vertically, whereas fibrils and fibers in the main part were oriented horizontally in the WF model (Figure 6a−d). In the NF model, no specific orientation was observed in either the vertical protrusion or the main part (Figure 6e−h). Comparing the collagen orientation average peak value with the horizontal orientation model of day 0 in the WF model, the main part in the vertical/horizontal orientation model had no significant difference (0.0169 ± 0.0027, Figure 6j) with that of the horizontal WF model (0.0161 ± 0.0026, Figure 2e). However, the vertical protrusions part in the vertical/horizontal orientation model tended to be lower (0.0124 ± 0.0021, Figure 6i) than in the horizontal orientation model. Interestingly, the fibrils and fibers were thinner in the vertical protrusion and thicker in the main part in both the WF and NF models (Figure 6m−p). Observing the main part, where the fiber grew noticeably, the WF model, with a longer-tailed distribution, formed fibers that were thicker than those of the NF model (Figure 6n,p). With both fibril and fiber thicknesses significantly thinner in the vertical protrusion part than in the main part (Figure 6m,n), the orientation of fibrils and fibers was evaluated with SEM images at a magnification of 80,000× (Figure S12a). The orientation value in the vertical protrusion part calculated from an SEM image with 80,000× magnification (0.0162 ± 0.0042, Figure S12b) was comparable to that of the horizontal orientation model. Thus, it is suggested that both the vertical and horizontal directions of this model are well-oriented, as in the horizontal orientation model. The mechanism of collagen orientation is thought to be due to the influence of flow and "walls" as in the horizontal orientation model. In our experiment, because the collagen flow stopped first at the vertical protrusion, it was considered to have gelated before the main part. As the vertical protrusion part is narrower than the horizontal, collagen forms "walls" more quickly in the vertical protrusion part, leading to faster completion of gelation. Consequently, fewer fibrils were produced in the vertical regions than in the horizontal regions, and the fibers

https://doi.org/10.1021/acsbiomaterials.4c02156
ACS Biomater. Sci. Eng. 2025, 11, 2875−2887

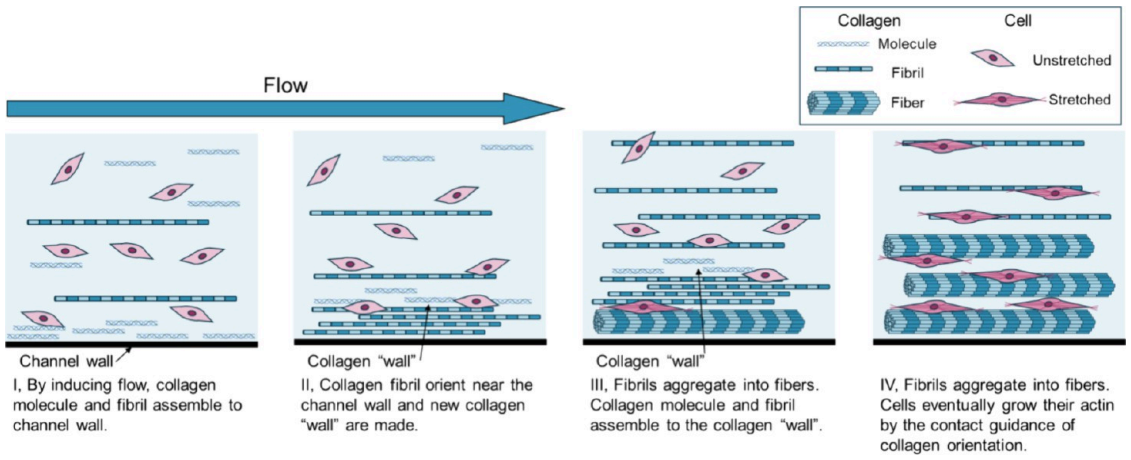

Figure 8. Schematic representation of the mechanism of collagen and cell orientation by flow. Collagen molecules and fibrils align parallel to the flow due to the influence of the flow and wall effect. This wall effect, starting from the outer channel wall, creates a gelated collagen "wall" toward the inside of the channel. Then, collagen fibrils aggregate into collagen fibers. As the cells proliferate, by responding to contact guidance of collagen fibrils and fiber orientation, focal adhesion and F-actin are activated and organize anisotropic traction forces, which, in turn, drive cell orientation.

aggregated by these fibrils were thinner in the vertical regions. This explains the thinner fibers in the vertical protrusion than those in the main part (Figure 6m,n). However, because the NF model was unaffected by this flow, neighboring fibrils were not parallel, and it was challenging to form thicker fibers, as explained in the horizontal orientation model. From the cell observations, cells were observed in the vertical protrusion part with a vertical orientation (Figure 7c,m), whereas the main part showed a horizontal orientation (Figure 7f,n). The cells were oriented by contact guidance of the collagen orientation.[35,36] Our fluidic device model suggests the ability to control both horizontal and fine vertical orientations. In addition, the WF model achieved a model in which the thicknesses were thinner in the vertical part and thicker in the main part, similar to human dermal skin. In the human papillary dermis, thinner collagen bundles are oriented vertically, whereas the reticular dermis has thicker collagen fiber bundles oriented horizontally.[12] In other words, it is possible that the collagen bundle thickness and orientation could be controlled by inducing flow.

To investigate the limitation of collagen diameter thickness, the effects of preparative conditions, such as flow rate, flow channel width, and incubation time, on the orientation and diameter of collagen fibrils and fibers were considered. For the flow rate, at 0.3 mL/h, collagen fibrils and fibers were less oriented and had smaller diameters than those at 3 mL/h (Figure S10). In contrast, there were no significant differences in the orientation and diameter of the collagen fibrils and fibers between 3 and 30 mL/h (Figure S10). This result indicated that 3 mL/h provided sufficient shear stress to the collagen fibrils and fibers for orientation. These results indicated that sufficient alignment was maintained when the collagen diameter ranged between 50 and 60 nm. Next, to observe the effect of channel width using two devices (2 × 3 mm and 1 × 1.5 mm), the inlet flow rate for the 1 × 1.5 mm device was set to 0.739 mL/h based on the multiple COMSOL simulations. Under these conditions, the flow velocity at the center of the device corresponds to 3 mL/h in the 2 × 3 mm device (Figure S13). SEM analysis (Figure S14) showed no significant differences in collagen fibril and fiber orientation; however, the smaller-width device produced thinner collagen fibrils and fibers. The influence of the channel width on the collagen diameter confirmed the principle of collagen orientation discussed in this study. Thus, the modes of collagen diameter ranged between 10 and 20 nm in the vertical protrusion part of our vertical/horizontal model (Figure 6m), which was the smallest diameter in our study and was affected by the small channel width. After 7 days, the highest mode reached 140−150 nm, with a maximum of 1.52 μm (Figure 3o). Our findings indicate that the collagen diameter can be controlled within 10−150 nm (mode) and up to 1.52 μm (maximum), while maintaining orientation. This range aligns with that of human tissues, including the dermis (50−70 nm),[40] cartilage (50−100 nm),[41] tendon fibrils (100 nm),[42] and tendon fibers (1−300 μm).[43]

In this study, micro-oriented and two-directional collagen models were fabricated with a flow channel using 3D printing, and the mechanism of cell alignment via collagen orientation was elucidated (Figure 8). To date, it has been challenging to form fine structures and simultaneously control their orientation in horizontal and vertical directions. By developing an experimental system using fluidic devices and 3D printing technology, we successfully controlled the size and direction of collagen fibrils, fibers, and cells. The microstructure of cell scaffolds is crucial for cell adhesion, proliferation, and contact guidance.[44] Oriented collagen hydrogels enhance mechanical properties and mimic cellular environments, having been applied in tissue repair and regeneration.[6] A skin model incorporating fibroblasts within a protrusion structure improved barrier function, basement membrane formation, and epidermal proliferation while maintaining differentiation.[45] As these protrusion structures diminish with age,[8] our model, which controls cell orientation within the protrusion structures, can replicate age-related and pathological changes in collagen ECM. Our model enables the evaluation of cosmetics and pharmaceuticals, and offers potential applications in tissue repair, transplantation, and safety assessments.

5. CONCLUSIONS

In this study, we developed a collagen tissue with multiscale and multidirectional controlled orientation using fluidic devices prepared using 3D printing technology. To date, the mechanism of orientation has not been well explained at the molecular level. However, our study carefully discussed the

https://doi.org/10.1021/acsbiomaterials.4c02156
ACS Biomater. Sci. Eng. 2025, 11, 2875−2887

principle of collagen orientation by observing collagen fibers on the nanoscale and focusing on collagen contraction. The orientation of the two cell types, fibroblasts and MSCs, suggests that this technology can be applied to various cell types. In the future, this system will lead to the customization of tissue-specific models using fine, multidirectionally oriented biomaterial scaffolds for the preparation of various oriented biological tissues.

■ ASSOCIATED CONTENT

Supporting Information

The Supporting Information is available free of charge at https://pubs.acs.org/doi/10.1021/acsbiomaterials.4c02156.

Collagen I-A solution viscosity; method of quantification of collagen and cell orientation; simulation with different inlet flow rates in horizontal orientation models; morphology of collagen hydrogels; simulation in vertical/horizontal orientation models; optimizing conditions of experimental flow rate of syringe pump; simulation to optimize the vertical/horizontal orientation models; high-magnification SEM observation of vertical/horizontal orientation models; effects of channel size on the orientation and diameter of collagen fibrils and fibers (PDF)

■ AUTHOR INFORMATION

Corresponding Author

Kazutoshi Iijima − *Faculty of Engineering and Institute of Advanced Sciences, Yokohama National University, Yokohama 240-8501, Japan;* orcid.org/0000-0001-9173-1666; Phone: +81-45-339-3997; Email: iijima-kazutoshi-mh@ynu.ac.jp; Fax: +81-44-339-3997

Authors

Mizuki Iijima − *Graduate School of Engineering Science, Yokohama National University, Yokohama 240-8501, Japan*

Mitsuki Sato − *Graduate School of Engineering Science, Yokohama National University, Yokohama 240-8501, Japan*

Hoshi Wakabayashi − *Graduate School of Engineering Science, Yokohama National University, Yokohama 240-8501, Japan*

Kaori Kojima − *Graduate School of Engineering Science, Yokohama National University, Yokohama 240-8501, Japan*

Kanata Togashi − *Graduate School of Engineering Science, Yokohama National University, Yokohama 240-8501, Japan*

Shogo Oishi − *Graduate School of Engineering Science, Yokohama National University, Yokohama 240-8501, Japan*

Takumi Misu − *Graduate School of Engineering Science, Yokohama National University, Yokohama 240-8501, Japan*

Masaru Mukai − *Faculty of Engineering, Yokohama National University, Yokohama 240-8501, Japan;* orcid.org/0000-0002-9508-3464

Hiroki Miyajima − *Faculty of Engineering, Yokohama National University, Yokohama 240-8501, Japan*

Shoji Maruo − *Faculty of Engineering, Institute of Advanced Sciences, and Institute for Multidisciplinary Sciences, Yokohama National University, Yokohama 240-8501, Japan*

Complete contact information is available at: https://pubs.acs.org/10.1021/acsbiomaterials.4c02156

Author Contributions

M.I., H.M., and K.I. made conceptualization. M.I., H.M., M.M., S.M., and K.I. designed the experiments. M.I. conducted cell culture, the fabrication of collagen models, and all analysis. M.S., K.K., and S.O. conducted the fabrication of master and PDMS mold. M.I., M.S., K.T., and T.M conducted the simulation by COMSOL. M.I. and H.W. conducted the fabrication of vertical/horizontal orientation models. M.I. drafted the original manuscript. K.I. reviewed and contributed to the revision of the manuscript drafts. All authors have given approval to the final version of the manuscript.

Funding

This study was funded by the Japan Science and Technology Agency (JST), CREST, Grant Number JPMJCR1905, Japan.

Notes

The authors declare no competing financial interest.

■ ACKNOWLEDGMENTS

SEM, fluorescence microscopy, and zoom microscopy were performed at the Instrumental Analysis Center of Yokohama National University.

■ REFERENCES

(1) Kardler, K. E.; Holmes, D. F.; Trotter, J. A.; Chapman, J. A. Collagen fibril formation. *Biochem. J.* **1996**, *316* (1), 1−11.

(2) Chung, H. J.; Uitto, J. Type VII collagen: the anchoring fibril protein at fault in dystrophic epidermolysis bullosa. *Dermatol Clin.* **2010**, *28* (1), 93−105.

(3) Ottani, V.; Raspanti, M.; Ruggeri, A. Collagen structure and functional implications. *Micron* **2001**, *32* (3), 251−260.

(4) Wolf, K.; Alexander, S.; Schacht, V.; Coussens, L. M.; Andrian, U. H.; Rheenen, J.; Deryugina, E.; Friedl, P. Collagen-based cell migration models in vitro and in vivo. *Semin. Cell Dev. Biol.* **2009**, *20* (8), 931−941.

(5) Eyre, D. R. Collagen: molecular diversity in the body's protein scaffold. *Science* **1980**, *207* (4437), 1315−1322.

(6) Zeng, R.; Tang, K.; Tian, H.; Pei, Y. Collagen materials with oriented structure for biomedical applications. *J. Polym. Sci.* **2024**, *62* (6), 998−1019.

(7) Birk, D. E.; Brückner, P. Collagens, Suprastructures, and Collagen Fibril Assembly. *Biol. Extracell. Matrix.* **2011**, 77−115.

(8) Lynch, B.; Pageon, H.; Le Blay, H.; Brizion, S.; Bastien, P.; Bornschlögl, T.; Domanov, Y. A mechanistic view on the aging human skin through ex vivo layer-by-layer analysis of mechanics and microstructure of facial and mammary dermis. *Sci. Rep.* **2022**, *12*, 849.

(9) Weiner, S.; Traub, W. Bone structure: from angstroms to microns. *FASEB J.* **1992**, *6* (3), 879−885.

(10) Elliott, D. H. Structure and function of mammalian tendon. *Biol. Rev. Camb. Philos. Soc.* **1965**, *40* (3), 392−421.

(11) Nakano, T.; Ishimoto, T.; Lee, J. W.; Umakoshi, Y. Preferential orientation of biological apatite crystallite in original, regenerated and diseased cortical bones. *J. Seramic. Soc. Jpn.* **2008**, *116*, 313.

(12) Marcos-Garcés, V.; Aguilar, P. M.; Serrano, C. B.; Bustos, V. G.; Seguí, J. B.; Izquierdo, A. F.; Ruiz-Saurí, A. Age-related dermal collagen changes during development, maturation and ageing - a morphometric and comparative study. *J. Anat.* **2014**, *225* (1), 98−108.

(13) Walters, B. D.; Stegemann, J. P. Strategies for directing the structure and function of three-dimensional collagen biomaterials across length scales. *Acta Biomater.* **2014**, *10* (4), 1488−1501.

(14) Guido, S.; Tranquillo, R. T. A methodology for the systematic and quantitative study of cell contact guidance in oriented collagen gels. Correlation of fibroblast orientation and gel birefringence. *J. Cell Sci.* **1993**, *105* (Pt 2), 317−331.

(15) Antman-Passig, M.; Shefi, O. Remote Magnetic Orientation of 3D Collagen Hydrogels for Directed Neuronal Regeneration. *Nano Lett.* **2016**, *16* (4), 2567−2573.
(16) Guo, C.; Kaufman, L. J. Flow and magnetic field induced collagen alignment. *Biomater.* **2007**, *28* (6), 1105−1114.
(17) Bürck, J.; Heissler, S.; Geckle, U.; Ardakani, M. F.; Schneider, R.; Ulrich, A. S.; Kazanci, M. Resemblance of Electrospun Collagen Nanofibers to Their Native Structure. *Langmuir.* **2013**, *29* (5), 1562−1572.
(18) Kimura, S.; Tsuchiya, A.; Ogawa, M.; Ono, M.; Suda, N.; Sekimoto, K.; Takeo, M.; Tsuji, T. Tissue-scale tensional homeostasis in skin regulates structure and physiological function. *Commun. Biol.* **2020**, *3*, 637.
(19) Nam, E.; Lee, W. C.; Takeuchi, S. Formation of Highly Aligned Collagen Nanofibers by Continuous Cyclic Stretch of a Collagen Hydrogel Sheet. *Macromol. Biosci.* **2016**, *16* (7), 995−1000.
(20) Buskermolen, A. B. C.; Ristori, T.; Mostert, D.; Turnhout, M. C.; Shishvan, S. S.; Loerakker, S.; Kurniawan, N. A.; Deshpande, V. S.; Bouten, C. V. C. Cellular Contact Guidance Emerges from Gap Avoidance. *Cell Rep. Phys. Sci.* **2020**, *1* (5), No. 100055.
(21) Lanfer, B.; Freudenberg, U.; Zimmermann, R.; Stamov, D.; Körber, V.; Werner, C. Aligned fibrillar collagen matrices obtained by shear flow deposition. *Biomater.* **2008**, *29* (28), 3888−3895.
(22) Lee, P.; Lin, R.; Moon, J.; Lee, L. P. Microfluidic alignment of collagen fibers for in vitro cell culture. *Biomed. Microdevices.* **2006**, *8* (1), 35−41.
(23) Kivanany, P. B.; Grose, K. C.; Yonet-Tanyeri, N.; Manohar, S.; Sunkara, Y.; Lam, K. H.; Schmidtke, D. W.; Varner, V. D.; Petroll, W. M. An In Vitro Model for Assessing Corneal Keratocyte Spreading and Migration on Aligned Fibrillar Collagen. *J. Funct Biomater.* **2018**, *9* (4), 54.
(24) Giacomini, F.; Barata, D. B.; Rho, H. S.; Birgani, Z. T.; Blitterswijk, C.; Giselbrecht, S.; Truckenmüller, R.; Habibović, P. Microfluidically Aligned Collagen to Maintain the Phenotype of Tenocytes In Vitro. *Adv. Healthc. Mater.* **2024**, *13* (6), No. 2303672.
(25) Batista, M. P.; Schroeter, B.; Fernández, N.; Gaspar, F. B.; do Rosário Bronze, M.; Duarte, A. R.; Gurikov, P. A Novel Collagen Aerogel with Relevant Features for Topical Biomedical Applications. *Chempluschem.* **2024**, *89* (7), No. e202400122.
(26) Rezakhaniha, R.; Agianniotis, A.; Schrauwen, J. T. C.; Griffa, A.; Sage, D.; Bouten, C. V. C.; van de Vosse, F. N.; Unser, M.; Stergiopulos, N. Experimental investigation of collagen waviness and orientation in the arterial adventitia using confocal laser scanning microscopy. *Biomech Model Mechanobiol.* **2012**, *11*, 461−473.
(27) Kanda, Y. Investigation of the freely available easy-to-use software 'EZR' for medical statistics. *Bone Marrow Transplant.* **2013**, *48*, 452−458.
(28) Ahmed, A.; Mansouri, M.; Joshi, I. M.; Byerley, A. M.; Day, S. W.; Gaborski, T. R.; Abhyankar, V. V. Local extensional flows promote long-range fiber alignment in 3D collagen hydrogels. *Biofabrication* **2022**, *14* (3), No. 035019.
(29) Attia, U. M.; Marson, S.; Alcock, J. R. Micro-injection moulding of polymer microfluidic devices. *Microfluid. Nanofluid.* **2009**, *7*, 1−28.
(30) Abdalkader, R.; Konishi, S.; Fujita, T. The Development of Biomimetic Aligned Skeletal Muscles in a Fully 3D Printed Microfluidic Device. *Biomimetics* **2022**, *7* (1), 2.
(31) Schwartz, J. J. Additive manufacturing: Frameworks for chemical understanding and advancement in vat photopolymerization. *MRS Bull.* **2022**, *47*, 628−641.
(32) Salih, N. M.; Hashim, U.; Nayan, N.; Soon, C. F.; Sahdan, M. Z. Numerical Simulation of Water Flow Velocity for Microfluidic Application Using COMSOL Multiphysics. *Adv. Mater. Res.* **2014**, *925*, 651−655.
(33) Schaart, J. M.; Lindert, M. K.; Roverts, R.; Nijhuis, W. H.; Sommerdijk, N.; Akiva, A. Cell-induced collagen alignment in a 3D in vitro culture during extracellular matrix production. *J. Struct. Biol.* **2024**, *216* (2), No. 108096.
(34) Marion, N. W.; Mao, J. J. Mesenchymal stem cells and tissue engineering. *Methods Enzymol.* **2006**, *420*, 339−361.
(35) Ray, A.; Lee, O.; Win, Z.; Edwards, R. M.; Alford, P. W.; Kim, D. H.; Provenzano, P. P. Anisotropic forces from spatially constrained focal adhesions mediate contact guidance directed cell migration. *Nat. Commun.* **2017**, *8*, 14923.
(36) Ray, A.; Provenzano, P. P. Aligned forces: Origins and mechanisms of cancer dissemination guided by extracellular matrix architecture. *Curr. Opin Cell Biol.* **2021**, *72*, 63−71.
(37) Kaverina, I.; Krylyshkina, O.; Small, J. V. Regulation of substrate adhesion dynamics during cell motility. *Int. J. Biochem. Cell Biol.* **2002**, *34* (7), 746−761.
(38) Jones, C. A.; Cibula, M.; Feng, J.; Krnacik, E. A.; McIntyre, D. H.; Levine, H.; Sun, B. Micromechanics of cellularized biopolymer networks. *Proc. Natl. Acad. Sci. U. S. A.* **2015**, *112* (37), E5117−E5122.
(39) Gjorevski, N.; Nelson, C. M. Mapping of mechanical strains and stresses around quiescent engineered three-dimensional epithelial tissues. *Biophys. J.* **2012**, *103* (1), 152−162.
(40) Barton, S. P.; Marks, R. Measurement of collagen-fibre diameter in human skin. *J. Cutan. Pathol.* **1984**, *11* (1), 18−26.
(41) Changoor, A.; Nelea, M.; Méthot, S.; Tran-Khanh, N.; Chevrier, A.; Restrepo, A.; Shive, M. S.; Hoemann, C. D.; Buschmann, M. D. Structural characteristics of the collagen network in human normal, degraded and repair articular cartilages observed in polarized light and scanning electron microscopies. *Osteoarthritis Cartilage* **2011**, *19* (12), 1458−1468.
(42) Erisken, C.; Zhang, X.; Moffat, K. L.; Levine, W. N.; Lu, H. H. Scaffold Fiber Diameter Regulates Human Tendon Fibroblast Growth and Differentiation. *Tissue Eng. Part A* **2013**, *19* (3−4), 519−528.
(43) Silver, F. H.; Kato, Y. P.; Ohno, M.; Wasserman, A. J. Analysis of mammalian connective tissue: relationship between hierarchical structures and mechanical properties. *J. Long Term Eff Med. Implants* **1992**, *2*, 165−198.
(44) Yañez-Soto, B.; Liliensiek, S. J.; Murphy, C. J.; Nealey, P. F. Biochemically and topographically engineered poly(ethylene glycol) diacrylate hydrogels with biomimetic characteristics as substrates for human corneal epithelial cells. *J. Biomed Mater. Res. Part A* **2013**, *101A*, 1184−1194.
(45) Blackstone, B. N.; Malara, M. M.; Baumann, M. E.; McFarland, K. L.; Supp, D. M.; Powell, H. M. Fractional CO2 laser micropatterning of cell-seeded electrospun collagen scaffolds enables rete ridge formation in 3D engineered skin. *Acta Biomater.* **2020**, *102*, 287−297.

https://doi.org/10.1021/acsbiomaterials.4c02156
ACS Biomater. Sci. Eng. 2025, 11, 2875−2887